A New GROMOS Force Field for Hexopyranose-Based Carbohydrates

ROBERTO D. LINS,[1] PHILIPPE H. HÜNENBERGER[2]
[1]*École Polytechnique Fédérale de Lausanne (EPFL), Laboratory of Computational Chemistry and Biochemistry, Institute of Chemical Sciences and Engineering, CH-1015 Lausanne, Switzerland*
[2]*Laboratorium für Physikalische Chemie, ETH-Hönggerberg, HCI, CH-8093 Zürich, Switzerland*

Received 3 March 2005; Accepted 10 May 2005
DOI 10.1002/jcc.20275
Published online in Wiley InterScience (www.interscience.wiley.com).

Abstract: A new parameter set (referred to as 45A4) is developed for the explicit-solvent simulation of hexopyranose-based carbohydrates. This set is compatible with the most recent version of the GROMOS force field for proteins, nucleic acids, and lipids, and the SPC water model. The parametrization procedure relies on: (1) reassigning the atomic partial charges based on a fit to the quantum-mechanical electrostatic potential around a trisaccharide; (2) refining the torsional potential parameters associated with the rotations of the hydroxymethyl, hydroxyl, and anomeric alkoxy groups by fitting to corresponding quantum-mechanical profiles for hexopyranosides; (3) adapting the torsional potential parameters determining the ring conformation so as to stabilize the (experimentally predominant) $^4C_1$ chair conformation. The other (van der Waals and nontorsional covalent) parameters and the rules for third and excluded neighbors are taken directly from the most recent version of the GROMOS force field (except for one additional exclusion). The new set is general enough to define parameters for any (unbranched) hexopyranose-based mono-, di-, oligo- or polysaccharide. In the present article, this force field is validated for a limited set of monosaccharides (α- and β-D-glucose, α- and β-D-galactose) and disaccharides (trehalose, maltose, and cellobiose) in solution, by comparing the results of simulations to available experimental data. More extensive validation will be the scope of a forthcoming article.

 J Comput Chem 26: 1400–1412, 2005

Key words: carbohydrate; hexopyranose; computer simulation; force field; molecular dynamics

Introduction

During the past decade, the scientific community has shown a renewed interest for the study of carbohydrates, triggered in large part by the recognition of their key role in many biochemical[1,2] and technological processes,[3] as well as their potential for the design of new materials.[3] In addition to their long-known structural and energetic role in living organisms,[4] carbohydrates are also involved in numerous biological processes such as coagulation, immune defense, cellular growth and adhesion, fertilization, inflammation, viral replication, and parasitic infection.[1,2,5,6]

The most important experimental techniques available to study carbohydrates are X-ray crystallography and nuclear magnetic resonance (NMR) spectroscopy.[7–9] However, due to the high intrinsic flexibility of di-, oligo-, and polysaccharides, these methods only provide limited information in the context of solvated carbohydrates, as opposed to other classes of biomolecules (e.g., proteins, nucleic acids) generally characterized by a well-defined dominant (native) conformation in solution. On the one hand, X-ray diffraction techniques (as applied to crystals or fibers) often provide structures of di-, oligo-, and polysaccharides at atomic resolution in the crystalline state.[10] However, the presence of crystal-packing forces, generally resulting in the dominance of a single molecular conformation, limit the relevance of solid-state structures for the interpretation of data in solution. On the other hand, NMR experiments provide information about carbohydrates in solution, but only in terms of averages over all the conformations at equilibrium on the time scale of the experiment.[11] For these reasons, the two techniques only enable a limited understanding of the structural and dynamical properties of solvated saccharides.[12] Many other experimental techniques (e.g., electron microscopy, light or neutron diffraction, infrared and Raman spectroscopy, optical rotation, fluorescence energy transfer, or

Correspondence to: P. H. Hünenberger; e-mail: phil@igc.phys.chem.ethz.ch

Contract/grant sponsor: Swiss National Foundation; contract/grant numbers: 21-63408 and 21-105397

rheological measurements) also provide useful, but even more indirect information about carbohydrates in solution.[7,13]

To overcome these limitations, modern theoretical methods are now being extensively used for the investigation of the structure, flexibility, and dynamics of saccharides. This approach has been so successful that theoretical methods are today no longer considered as a mere complement to experimental measurements, but as essential tools for a complete understanding of the physicochemical properties of carbohydrates.[14,15]

Yet the modeling of carbohydrate has been somewhat lagging behind that of other biomolecules, mainly because these compounds constitute a real challenge for the design of molecular models. This is, in particular, due to: (1) their amazing structural diversity (wide spectrum of monomeric units and linkage types); (2) their high content of vicinal hydroxyl group (many possible rotamer combinations, high polarity); (3) their high flexibility in solution (multiple conformers at equilibrium); (4) the interplay between complex effects in determining their conformational preferences in solution (steric, stereoelectronic, solvation, and entropic effects); (5) the scarcity of high-resolution experimental data for model refinement.

Our interest lies primarily in performing long time scale simulations of large oligo- and polysaccharides in the condensed phase, to investigate their interactions with the solvent, with other carbohydrates and with other classes of biomolecules. For such systems, quantum-mechanical methods are computationally far too demanding, and the only feasible alternative is the use of classical force fields in combination with molecular dynamics (MD) simulations. However, the proper description of the structural, conformational, and dynamical properties of carbohydrates requires the use of a high-quality and consistently parametrized force field. Although several carbohydrate force fields for explicit-solvent simulations have been developed in the past few years,[16] including CHARMM,[17–19] AMBER,[20–24] OPLS,[25–27] and GROMOS,[28–32] to mention only a few, there still appears to be room for improvement.[33,34] For example, a systematic test of 20 different force fields for carbohydrates[33] revealed that the agreement among the descriptions provided by the different parameter sets is confined to the lowest energy conformers up to the disaccharide level only. It is suggested that large differences in the sampled conformational ensembles arise from the fact that force fields have been developed to account for the properties of a selected (limited) set of small molecules, aiming to predict molecular properties for which there is often a lack of accurate experimental data. Thus, the use of a specific force field only enables the proper representation of a certain class of carbohydrates.

The development of a high-quality parameter set for carbohydrates that is, in addition, compatible with a general force field for biomolecules (proteins, nucleic acids, and lipids) constitutes the main goal of the present work. It has been chosen here to enforce compatibility with the GROMOS96 functional form and force field parameters,[29,35] and the SPC water model.[36] The original 43A1 version of the GROMOS96 force field[29] has been recently refined and validated against experimental and quantum-mechanical data in the context of: (1) pure alkanes[37,38] (torsional and third-neighbor van der Waals interaction parameters); (2) alkane-water systems[38] (van der Waals interaction parameters); (3) lipids[39] (charges and torsional interaction parameters); (4) nucleic acids[40] (explicit aromatic hydrogen atoms, charges, and torsional interaction parameters); (5) interaction between polar groups[41] (choice of hydrogen-bonding vs. nonhydrogen-bonding van der Waals repulsion parameters). The force field incorporating the two former modifications is referred to as the 45A3 force field.[37,38] However, simple tests using the GROMOS carbohydrate force field, either based on the original 43A1 parameter set[31,32,42,43] or on the 45A3 parameter set (unpublished data), have shown a strong underestimation of the anomeric effect and incorrect dihedral-angle distributions in simple di- and oligosaccharides, sometimes including distorted ring conformations. The required refinement of the GROMOS force field (mainly charges and torsional interaction parameters) in the context of hexopyranose-based carbohydrates is the goal of the present work. The updated version of the GROMOS force field, including the five changes listed above and the presently derived set of carbohydrate parameters, will be referred to as the GROMOS 45A4 force field. This new version of the force field should, in particular, enable the study by molecular simulation of carbohydrates in solution as well as of their interactions with other classes of biomolecules.

Force-Field Parametrization

Parametrization Strategy

Staring from the GROMOS96 functional form[29,35] and the 45A3 parameters for bond stretching, bond-angle bending, improper-dihedral deformation and van der Waals interactions (including the modifications previously reported for aliphatic carbons[37,38]), a new set of charges and torsional interaction potentials is developed for hexopyranose-based carbohydrates. The parameter derivation relies exclusively on fitting to quantum-mechanical data, based on the following strategy:

1. The definition of atom types (including united-atom aliphatic CH, CH_2, and CH_3 groups) and the corresponding van der Waals interaction parameters are taken directly from the GROMOS 45A3 force field.[37,38]
2. The atomic partial charges are primarily obtained by fitting the electrostatic potential outside a cellotriose molecule ($\beta(1 \rightarrow 4)$-linked D-glucopyranose trisaccharide) to the potential obtained from quantum-mechanical calculations (with aliphatic hydrogen charges constrained to zero), followed by a limited charge redistribution permitting the definition of neutral charge groups and the use of identical charges for all carbon-hydroxyl groups (except the lactol group).
3. The nontorsional covalent interaction parameters (bond stretching, bond-angle bending and improper-dihedral deformation) are taken directly from the GROMOS 45A3 force field[37,38] (these specific parameters are also unaltered with respect to the 43A1 set[29]).
4. The torsional dihedral potentials associated with the rotations of the hydroxymethyl group, all hydroxyl groups and the anomeric alkoxy group are obtained by fitting the corresponding classical energy profiles to energy profiles obtained from quantum-mechanical calculations on α- and β-*O*-methyl-D-glucopyranoside as well as β-*O*-methyl-D-galactopyranoside, followed by lim-

ited changes to obtain identical torsional interaction parameters for all hydroxyl groups (except the lactol group). The torsional dihedral potentials determining the conformation of the hexopyranose ring are slightly adapted from the 45A3 force field,[37,38] to enhance the stability of the $^4C_1$ chair conformation.
5. The definition of excluded atoms matches the GROMOS convention[29] (first and second covalent neighbors), with a single exception (the hydroxyl hydrogen atom of an unfunctionalized lactol group is excluded from its third-neighbor ring oxygen). The application of modified third-neighbor van der Waals interaction parameters matches the GROMOS convention[29] (all third covalent neighbors rely on a special set of repulsive van der Waals parameters).

The resulting force field is validated for a small set of mono- and disaccharides in solution, by comparing the results of explicit-solvent MD simulations to available experimental data from X-ray crystallography and NMR spectroscopy. This validation is currently limited to α- and β-D-glucose, α- and β-D-galactose, and the disaccharides α,α-trehalose (D-Glc*p*-$\alpha(1 \rightarrow 1')\alpha$-D-Glc*p*), β-maltose (D-Glc*p*-$\alpha(1 \rightarrow 4)$-β-D-Glc*p*), and β-cellobiose (D-Glc*p*-$\beta(1 \rightarrow 4)$-β-D-Glc*p*).

Atomic Partial Charges

The charge set developed for the new 45A4 carbohydrate force field is based on the fitting of the classical electrostatic potential outside a molecule to the corresponding quantum-mechanical potential, using the restrained electrostatic potential fit (RESP) procedure.[44,45] Previous applications of this method to derive charge sets for carbohydrate force fields have often primarily relied on the isolated glucopyranose or *O*-methyl-glucopyranoside molecule as a model compound.[15,17,46] However, in (unbranched) di-, oligo-, and polysaccharides, all nonterminal residues have two hydroxyl groups (including the lactol group) functionalized into a glycosidic bond. Such a modification in the chemical environment of these groups is expected to significantly alter their electronic properties (change density), and thus, the corresponding optimal atomic charges. To address this problem, Hartree–Fock (HF) calculations were performed on the cellotriose molecule ($\beta(1 \rightarrow 4)$-linked D-glucopyranose trisaccharide) at the 6-31G* level, starting from an initial configuration with ϕ (O_5–C_1–O_1–C_4') at 300° and ψ (C_1–O_1–C_4'–C_3') at 120° (see Fig. 1c for the atom numbering), and with all the hydroxyl groups oriented counterclockwise (as seen from the β-side of the ring; see conformation *A* in Fig. 1a). A full geometry optimization of this compound was followed by a RESP fitting using the NWChem4.1 program,[47] to obtain an initial set of partial charges. For these calculations, the charges of the aliphatic hydrogen atoms were constrained to zero, the dipole moment of the molecule was constrained to its quantum-mechanical value, and values of 0.005 a.u. for the harmonic and 0.001 a.u. for the hyperbolic restraints were used. The charges of topologically similar atoms within the central glucopyranose unit were then averaged. More precisely, only six distinct (averaged) charge values were retained to characterize the four atom sets $\{C_n | \; n = 1, 2, 3, 4, 6\}$, $\{O_n | \; n = 2, 3, 6\}$, $\{H_n | \; n = 2, 3, 6\}$ and $\{O_4, O_1\}$, and the two atoms C_5 and O_5 (see Fig. 1c for the atom numbering). Some further charge redistribution was required to permit the definition of neutral charge groups of restricted sizes within the molecule. These changes were very limited and did not significantly alter the quality of the electrostatic potential fit, but led to GROMOS-compatible and easily transferable parameters. In particular, the definition of carbon-hydroxyl group building blocks (CH—O—H and CH_2—O—H) with a zero net charge is very convenient for the extension of the force field to other monosaccharide units. The charge set for an unfunctionalized C_4–O_4–H_4 group (chain initiation patch), which is topologically similar to the other C_n–O_n–H_n (n = 2, 3, 6) groups, was taken directly from this carbon-hydroxyl group building block.

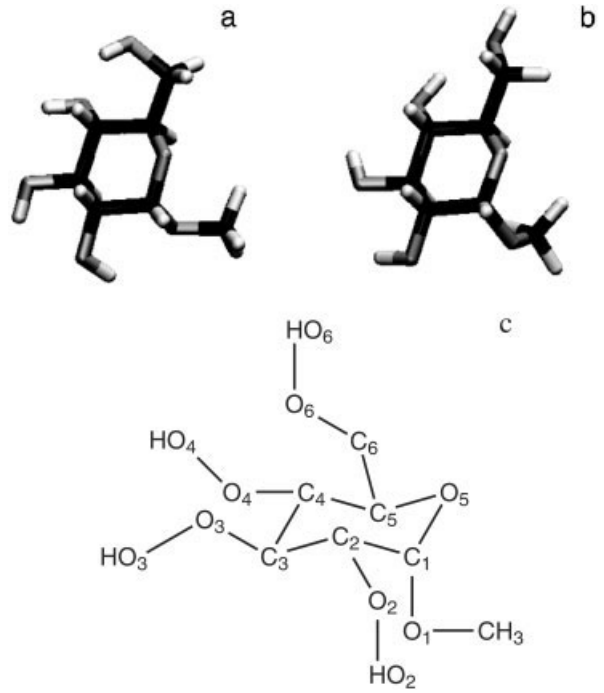

Figure 1. Structures of the two lowest energy conformers of α-*O*-methyl-D-glucopyranoside in vacuum (a,b), and atom numbering in the molecule (c). The two conformers represented, referred to as *A* (a) and *B* (b), were considered for the comparison of quantum-mechanical and molecular-mechanical torsional energy profiles during the optimization of the 45A4 torsional interaction parameters (Fig. 2).

Charge sets for residues involving an unfunctionalized C_1–O_1–H_1 (or a methyl-substituted C_1–O_1–CH_3) lactol group (chain termination patch) were obtained from a similar RESP fitting procedure carried out for a single β-D-glucopyranose (or β-*O*-methyl-D-glucopyranoside) unit, and constraining the charges of all atoms except O_1 and H_1 (or the methyl carbon, the charges of the methyl hydrogens being constrained to zero) to the previously determined values. Finally, charges for the C_1–O_1–$(1 \rightarrow 1')$-Hex*p*′ termination patch, where Hex*p* is an arbitrary hexopyranose, were obtained by considering the model compound α, α-trehalose (D-Glc*p*-$\alpha(1 \rightarrow 1')\alpha$-D-Glc*p*). A similar RESP fitting was carried out for this compound using the charges of the atoms O_5, C_1, O_1, C_1', and O_5' as free parameters, the charges of all other atoms being constrained to the previously derived values for the generic hexopyranose unit (except for a tiny adjustment of the C_5

and C'_5 charges, to enforce the neutrality of the above group of atoms).

At this point, it is important to mention that the definition of excluded atoms in the new 45A4 force field (i.e., atoms pairs for which the minimum-image nonbonded interaction is omitted) matches the GROMOS convention[29] (first and second covalent neighbors), with a single exception. In the presence of an unfunctionalized lactol group (reducing C_1–O_1–H_1 terminal group), the O_1 (lactol), and O_5 (ring) oxygens are excluded (second) neighbors. This implies in particular that they are not subject to van der Waals repulsion. For this reason, nothing prevents the positively charged hydrogen H_1 attached to O_1 to collapse with the negatively charged ring oxygen O_5, a situation that was indeed found to occur in some of our simulations. To remedy this problem, it was found necessary to also exclude the hydrogen atom H_1 of an unfunctionalized lactol group from interaction with its (third-neighbor) ring-oxygen atom O_5. A similar situation has been previously encountered in the GROMOS force field for the nucleic acid base adenine (and solved similarly by excluding atoms H61 and H62 from atom N7[40,48]).

The final 45A4 charge set for hexopyranose-based carbohydrates, to be used for (unbranched) mono-, di-, oligo-, and polysaccharides (including chain initiation and termination patches) is reported in Table 1, together with the corresponding charges in the 45A3 parameter set[37,38] (the charges of the 45A3 set are identical to those of the 43A1 set[29]). The charges are listed in the particular context of a (1 → 4)-linked hexopyranose monomer, but the description is easily adapted to units involved in (1 → 2)-, (1 → 3)-, or (1 → 6)-linkages. The (1 → 1)-linkage is implemented through the C_1–O_1–(1 → 1′)-Hex*p*′ termination patch.

Comparison between the GROMOS 45A3 and the new 45A4 charge sets reveals only moderate differences, the new charges being in general slightly higher compared to the original ones. This qualitative agreement is particularly interesting because the previous GROMOS charge sets (43A1, 43A2, and 43A3) have been derived primarily by fitting to thermodynamical properties of pure liquids and aqueous solutions, rather that to quantum-mechanical electrostatic potentials. However, a similar agreement has been previously noted for the dimethylphosphate and trimethylamine molecules during the refinement of the GROMOS lipid force field.[39] To further evaluate the realism of the present RESP-derived charges for the carbon-hydroxyl group building block in the context of intermolecular interactions in solution, these charges were used to define a new model for the ethanol molecule (C_{Me}: $0.0e$, C: $0.232e$, O: $-0.642e$, and H: $0.410e$), referred to here as the 45A4 ethanol model. The simulated pure liquid and aqueous solvation properties based on this model are compared to those of the 45A3 (same as 43A1) ethanol model[29] (C_{Me}: $0.0e$, C: $0.150e$, O: $-0.548e$, and H: $0.398e$) and to experimental data in Table 2. Although a charge set developed specifically for carbohydrates should not necessarily be expected to provide an accurate model for ethanol, the 45A4 ethanol model turns out to be surprisingly good. It represents a clear improvement over the 45A3 model in terms of density and hydration free energy, although the heat of vaporization is overestimated by 11% (while it is underestimated by 6% in the 45A3 model).

Table 1. Atomic Partial Charges of the New 45A4 Force Field for Hexopyranose-Based Carbohydrates, Compared to Those of the 45A3 Parameter Set.[37,38]

Atom	Type	45A4 charge [*e*]	45A3 charge [*e*]	CG end
4-OH initiation patch				
HO4	H	0.410	0.398	
O4	OA	−0.642	−0.548	
(*C*4)	CH_1	0.232	0.150	*
Monomeric unit [→ 4)-Hex*p*-1(]				
C4	CH_1	0.232	0.160	*
C3	CH_1	0.232	0.150	
O3	OA	−0.642	−0.548	
HO3	H	0.410	0.398	*
C2	CH_1	0.232	0.150	
O2	OA	−0.642	−0.548	
HO2	H	0.410	0.398	*
C6	CH_2	0.232	0.150	
O6	OA	−0.642	−0.548	
HO6	H	0.410	0.398	*
C5	CH_1	0.376	0.160	
O5	OA	−0.480	−0.360	
C1	CH_1	0.232	0.400	
O1	OA	−0.360	−0.360	
1-OH termination patch				
(*C*5)	CH_1	0.376	0.200	
(*C*1)	CH_1	0.232	0.310	
*O*1	OA	−0.538	−0.548	
HO1	H	0.410	0.398	*
1-OCH_3 termination patch				
C_{Me}	CH_3	0.232	—	*
1 → 1′-Hex*p*′ termination patch				
*C*5	CH_1	0.378	—	
*O*5, *O*5′	OA	−0.450	—	
*C*1, *C*1′	CH_1	0.242	—	
*O*1	OA	−0.340	—	
*C*5′	CH_1	0.378	—	*

A star in the last column indicates an atom terminating a (neutral) charge group (CG; center defined as the center of geometry of the atoms involved[29]). The charge set is reported in the particular context of a (1 → 4)-linked hexopyranose unit, but the table is easily adapted to (1 → 2)-, (1 → 3)-, or (1 → 6)-linkages. A monosaccharide molecule or the first residue in an unbranched di-, oligo-, or polysaccharide sequence must be initiated by a 4-OH initiation patch, requiring the indicated modifications. A monosaccharide molecule or the last residue in an unbranched di-, oligo-, or polysaccharide sequence must be terminated by a 1-OH, a 1-OCH_3 or a 1 → 1′-Hex*p*′ (i.e., a (1 → 1′)-linkage as, for example, in the disaccharide trehalose) termination patch, requiring the indicated modifications. Modifications may involve the insertion of additional atoms with specified charges (atom name in plain text), or a change in the charge of existing atoms (atom name in italics; parentheses indicate a charge change solely required in the 45A3 force field). For the 1 → 1′-Hex*p*′ termination patch, only the atoms involved in the linkage are listed. The charges of the atoms and charge-group definitions in the (1 → 1′)-linked hexopyranose unit itself are identical to those of the corresponding generic Hex*p*′ residue. The rules for excluded atoms and third-neighbors follow the GROMOS conventions,[29] except for an additional exclusion between the ring oxygen O_5 and the lactol hydrogen H_1 in residues terminated by a 1-OH patch.

Table 2. Comparison of Simulated Pure Liquid and Aqueous Solvation Properties for the 45A3 and 45A4 Ethanol Models with Experimental Results.[89,90]

	45A4	45A3	Experiment
ρ [g · cm^{-3}]	0.783	0.763	0.785
ΔH_{vap} [kJ · mol^{-1}]	47.0	39.8	42.3
ΔG_{hyd} [kJ · mol^{-1}]	−18.0	−13.0	−20.5

The quantities reported are the density ρ, heat of vaporization ΔH_{vap}, and hydration free energy ΔG_{hyd} (using the SPC water model[36]) at 300 K and 1 bar (these calculations were performed as described elsewhere[48]).

Covalent Interaction Parameters

The nontorsional covalent interaction parameters used in the new 45A4 force field for hexopyranose-based carbohydrates are taken directly from the GROMOS 45A3 force field[37,38] (these specific parameters are also unaltered with respect to the 43A1 parameter set[29]). The corresponding values are listed in Table 3 for reference.

The functional form of the potential-energy term associated with the stretching of bond m is given by

$$V_{b,m} = (1/4)k_{b,m}[b_m^2 - b_{o,m}^2]^2, \quad (1)$$

where b_m is the actual bond-length distance, b_o its reference value and $k_{b,m}$ the corresponding (quartic) force constant. Such a term is applied to all unique pairs of covalently linked atoms in the compound that match the pair of atom types specified in Table 3.

The functional form of the potential-energy term associated with the bending of bond angle m is given by

$$V_{\theta,m} = (1/2)k_{\theta,m}[\cos\theta_m - \cos\theta_{o,m}]^2, \quad (2)$$

where θ_m is the actual bond-angle value, θ_o its reference value and $k_{\theta,m}$ the corresponding (cosine-harmonic) force constant. Such a term is applied to all unique triplets of covalently linked atoms in the compound that match the sequence of atom types specified in Table 3.

The functional form of the potential-energy term associated with the deformation of improper-dihedral angle m is given by

$$V_{\xi,m} = (1/2)k_{\xi,m}[\xi_m - \xi_{m,o}]^2, \quad (3)$$

where ξ_m is the actual improper-dihedral angle value, ξ_o its reference value and $k_{\xi,m}$ the corresponding (harmonic) force constant. Such a term is only applied, for each hexopyranose monomer within the compound, to the subset of improper-dihedral angles specified in Table 3. The five terms in the list enforce a tetrahedral geometry around the successive C_n (n = 1, 2, 3, 4, 5) united-atom aliphatic carbons within the pyranose ring. The specific atom sequences reported in the table correspond to the stereochemistry of β-D-glucopyranose (hydroxymethyl group and all hydroxyl groups equatorial in the $^4C_1$ chair conformation). Inversion of the configuration around one or more centers (to generate the corresponding terms for the 31 other α or β anomers of the D or L enantiomers of all hexopyranoses) requires an inversion in the order of the second and third atoms in the corresponding listed sequence.

In contrast to other covalent interaction parameters, the torsional parameters were reoptimized specifically for application to hexopyranose-based carbohydrates. The functional form of the potential energy term associated with the torsion around dihedral angle m is given by

$$V_{\phi,m} = k_{\phi,m}[1 + \cos\delta_m\cos(n_m\phi_m)], \quad (4)$$

where ϕ_m is the actual dihedral-angle value, n_m the multiplicity of the term, δ_m the associated phase shift, and $k_{\phi,m}$ the corresponding force constant. Terms of this form are applied, for each hexopyranose monomer, to a subset of dihedral angles specified in a list (Table 4). Note, however, that a given dihedral angle may be involved in more than one torsional potential energy term with different multiplicities.

The hydroxyl and hydroxymethyl torsional parameter set of the new 45A4 force field is based on fitting the classical energy

Table 3. Bond Stretching, Bond-Angle Bending, and Improper-Dihedral Deformation Parameters Used in the 45A4 Force Field for Hexopyranose-Based Carbohydrates.

Bond type	k_b [10^6 kJ · mol^{-1} · nm^{-4}]	b_o [nm]
C–C	5.43	0.1520
C–O	6.10	0.1435
O–H	15.7	0.1000
Bond-angle type	**k_θ [kJ · mol^{-1}]**	**θ_o [deg]**
C–C–C	285	109.5
C–C–O	320	109.5
O–C–O	320	109.5
C–O–C	380	109.5
C–O–H	450	109.5
Improper-dihedral (β-D-Glc$p$)	**k_ξ [kJ · mol^{-1} · deg^{-2}]**	**ξ_o [deg]**
C_1–O_1–O_5–C_2	0.102	35.26439
C_2–O_2–C_3–C_1	0.102	35.26439
C_3–O_3–C_2–C_4	0.102	35.26439
C_4–C_3–O_4–C_5	0.102	35.26439
C_5–O_5–C_6–C_4	0.102	35.26439

The parameters refer to eqs. (1), (2), and (3). Bond-stretching terms are applied to all covalently linked atom pairs matching the pair of atom types specified in the table. Bond-angle bending terms are applied to all covalently linked atom triplets matching the sequence of atom types specified in the table. Improper-dihedral deformation terms are only applied, for each hexopyranose monomer, to the specified subset of improper-dihedral angles (see Fig. 1c for the numbering). The improper-dihedral terms are reported for the specific stereochemistry of β-D-glucopyranose. Inversion of the configuration at one or more centers (to generate the corresponding terms for the 31 other hexopyranoses) requires an inversion in the order of the second and third atoms in the corresponding sequence.

Table 4. Torsional Dihedral Interaction Parameters Used in the New 45A4 Force Field for Hexopyranose-Based Carbohydrates.

Dihedral angle	k_ϕ [kJ · mol^{-1}]	cos δ	n
C_2–C_1–O_5–C_5	3.77	+1	3
C_4–C_5–O_5–C_1	3.77	+1	3
C_1–C_2–C_3–C_4	5.92	+1	3
C_2–C_3–C_4–C_5	5.92	+1	3
C_3–C_2–C_1–O_5	5.92	+1	3
C_3–C_4–C_5–O_5	5.92	+1	3
O_1–C_1–C_2–O_2	2.09	+1	2
O_2–C_2–C_3–O_3	2.09	+1	2
O_3–C_3–C_4–O_4	2.09	+1	2
C_3–C_2–C_1–O_1	0.418	+1	2
C_4–C_3–C_2–O_2	0.418	+1	2
C_1–C_2–C_3–O_3	0.418	+1	2
C_5–C_4–C_3–O_3	0.418	+1	2
C_2–C_3–C_4–O_4	0.418	+1	2
C_6–C_5–C_4–O_4	0.418	+1	2
C_3–C_2–C_1–O_5	0.418	+1	2
C_3–C_4–C_5–O_5	0.418	+1	2
O_5–C_5–C_6–O_6[a] ($\tilde{\omega}$)	9.50	+1	3
O_5–C_5–C_6–O_6[a] ($\tilde{\omega}$)	9.35	−1	1
O_5–C_5–C_6–O_6[b] ($\tilde{\omega}$)	7.69	+1	3
O_5–C_5–C_6–O_6[b] ($\tilde{\omega}$)	6.66	−1	1
C_4–C_5–C_6–O_6[b] (ω)	2.67	−1	1
C_1–C_2–O_2–H_2 (χ_2)	3.90	+1	3
C_2–C_3–O_3–H_3 (χ_3)	3.90	+1	3
C_3–C_4–O_4–H_4 (χ_4)	3.90	+1	3
C_5–C_6–O_6–H_6 (χ_6)	3.90	+1	3
O_5–C_1–O_1–H_1, C′[c] (ϕ)	3.65	1	3
O_5–C_1–O_1–H_1, C′[c] (ϕ)	9.45	−1	1
O_5–C_1–O_1–H_1, C′[d] (ϕ)	4.69	1	3
O_5–C_1–O_1–H_1, C′[d] (ϕ)	3.41	−1	1

The parameters refer to eq. (4). Torsional dihedral potential terms are only applied, for each hexopyranose monomer, to the specified subset of torsional dihedral angles (see Fig. 1c for the numbering). Legend: [a]term to be used when the O_4 and C_6 atoms are on opposite sides of the ring plane (i.e., equatorial-equatorial or axial-axial, as, e.g., in glucose); [b]term to be used when the O_4 and C_6 atoms are on the same side of the ring plane (i.e., equatorial-axial or axial-equatorial, as, e.g., in galactose); [c]term to be used for the α anomer; [d]term to be used for the β anomer.

profiles for the rotation around specific dihedral angles (including the effects of electrostatic, van der Waals, and torsional dihedral interactions, and based on the new charge set of Table 1) to corresponding profiles computed using quantum-mechanical calculations. This fitting was performed primarily for the model compound α-*O*-methyl-D-glucopyranoside, considering the dihedral angles ϕ (O_5–C_1–O_1–CH_3), the four dihedral angles χ_n (C_{n-1}–C_n–O_n–H_n, n = 2, 3, 4, 6), and the dihedral angle $\tilde{\omega}$ (O_5–C_5–C_6–O_6), following the IUPAC definitions[49] except for $\tilde{\omega}$ (ω is defined as C_4–C_5–C_6–O_6, so that $\tilde{\omega} \approx \omega - 120°$ for hexopyranoses with an *R* configuration at C_5, such as glucose and galactose). The calculation for the dihedral angle ϕ was also carried out for β-*O*-methyl-D-glucopyranoside, and the calculation for the dihedral angles χ_4 and $\tilde{\omega}$ for α-*O*-methyl-D-galactopyranoside.

In vacuum, α-*O*-methyl-D-glucopyranoside presents two most stable conformations characterized by the highest number of intramolecular hydrogen bonds, and differing by the relative orientation of the hydroxyl groups around the ring (Fig. 1a and b). Both conformers were taken into account during the derivation of the torsional energy profiles. Conformation *A* (Fig. 1a) is characterized by a counterclockwise orientation of the hydroxymethyl, hydroxyl, and methoxy groups around the ring (as seen from its β-side) leading to four intramolecular hydrogen bonds. Conformation *B* (Fig. 1b) is characterized by a clockwise orientation of the hydroxymethyl and hydroxyl groups (but not of the methoxy group), leading to three intramolecular hydrogen bonds. In agreement with previous quantum-mechanical calculations,[50,51] the former conformation is energetically more stable (by about 13 kJ · mol^{-1} at the present HF/6-31G* level of theory).

The quantum-mechanical torsional profiles for the rotations around the hydroxymethyl, the four hydroxyl and the methoxy groups in α-*O*-methyl-D-glucopyranoside, as well as some additional profiles for β-*O*-methyl-D-glucopyranoside and α-*O*-methyl-D-galactopyranoside, were determined independently by increments of 30° at the HF/6-31G* level using the program Gaussian98.[52] Each single-point calculation involved starting from the fully optimized conformation *A* or *B* (Fig. 1), rotating the selected dihedral angle to its target value, and then fully reoptimizing all other degrees of freedom. In this way, two sets of quantum-mechanical energy profiles were generated for each dihedral angle, corresponding to an initial conformation of either type *A* or type *B*. The target quantum-mechanical profile used as a reference for the fitting of the force-field torsional parameters was determined by combining the lowest energy points from both the *A* and *B* profiles. The same procedure was repeated at the molecular-mechanical level using fully optimized structures (conjugate-gradient minimizer of GROMOS) with a harmonic dihedral-angle restraining potential of force constant 10 kJ · mol^{-1} · deg^{-2} on the specific dihedral angle. The differences between quantum-mechanical and molecular-mechanical profiles were fitted by cosine series, which served to determine the required changes in force field torsional parameters. However, for the sake of simplicity and transferability (at the expense of a slight reduction in the accuracy of the fit), a common torsional potential was selected for the four dihedral angles χ_n (n = 2, 3, 4, 6), while different parameters were retained for ϕ and $\tilde{\omega}$. The resulting optimized set of torsional parameters is reported in Table 4, while the comparison between the quantum-mechanical and corresponding molecular-mechanical profiles is shown in Figure 2.

At the quantum-mechanical level, the dihedral angles involving hydroxyl groups (χ_n, n = 2, 3, 4) generally present energy minima in the *gauche*+ (60°), *trans* (180°) and *gauche*− (300°) conformations (Fig. 2c–e). To reproduce this trend in the molecular-mechanical profiles, a common threefold torsional potential with phase-shift cosine +1 (favoring the three staggered conformations) was used for all hydroxyl groups, the force constant being selected by averaging over the optimal values derived for χ_2, χ_3, and χ_4. The resulting force constant (3.9 kJ · mol^{-1}) is significantly larger than the corresponding value used in the original 45A3 parameter set for these dihedral angles (1.26 kJ · mol^{-1}). Note also that the 45A3 parameter set[37,38] employed a different force constant for the χ dihedral angle of a hydroxyl group func-

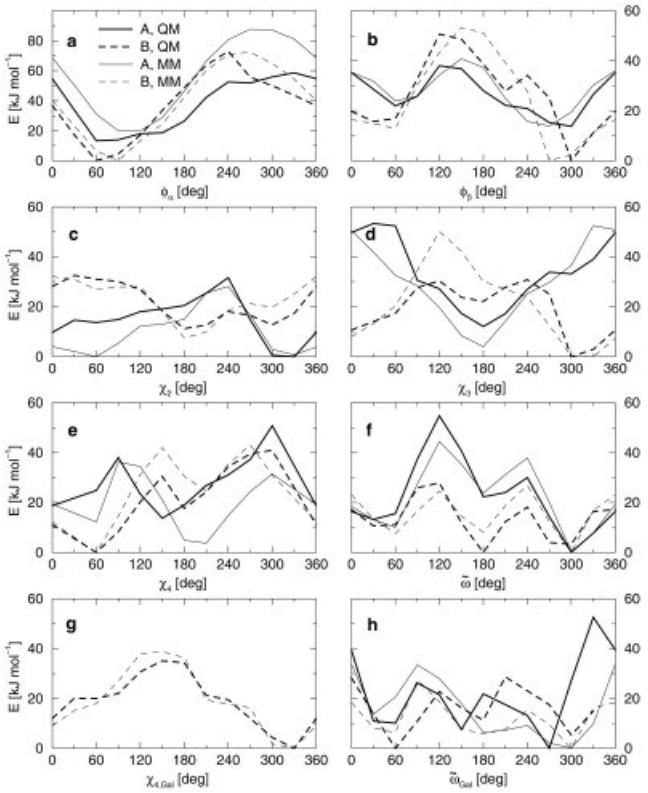

Figure 2. Comparison of the quantum-mechanical (QM) and molecular-mechanical (MM; based on the optimized 45A4 parameter set as reported in Tables 1, 3, and 4) torsional energy profiles for the rotation around the hydroxymethyl, the different hydroxyl and the methoxy groups in α-*O*-methyl-D-glucopyranoside (a,c–f), β-*O*-methyl-D-glucopyranoside (b), and α-*O*-methyl-D-galactopyranoside (g,h). The QM and MM profiles are reported for fully optimized conformations generated starting from either the *A* or *B* conformers (Fig. 1a and b) of the monosaccharide. For each method (QM or MM), energies are given relative to the minimum-energy point of either the *A* or *B* profile. The definition of the dihedral angles is ϕ (O_5–C_1–O_1–CH_3), χ_n (C_{n-1}–C_n–O_n–H_n, $n = 2, 3, 4$), and $\tilde{\omega}$ (O_5–C_5–C_6–O_6).

tionalized into a glycosidic bond (i.e., the ψ glycosidic dihedral angle), namely 3.77 kJ · mol^{-1}. This distinction is no longer retained in the new 45A4 force field.

The orientation of the methoxy group around the glycosidic dihedral angle ϕ is strongly influenced by the anomeric effect. As a consequence, the torsional profile for the corresponding rotation presents only one energy minimum in *gauche*+ for the α anomer and a predominant minimum in *gauche*− for the β anomer (Fig. 2a, and b). This trend is enforced in the molecular-mechanical profile by a combination of a threefold torsional potential with phase-shift cosine +1 (favoring the three staggered conformations; force constants 3.65 and 4.69 kJ · mol^{-1} for the α- and β-anomers, respectively), and a onefold potential with phase-shift cosine −1 (favoring the *cis* conformation; force constants 9.45 and 3.41 kJ · mol^{-1} for the α- and β-anomers, respectively). These combined torsional potentials replace the single threefold potential with force constant 3.77 kJ · mol^{-1} used in the 45A3 force field.

The rotational profile around the dihedral angle $\tilde{\omega}$ determining the orientation of the hydroxymethyl group in α-*O*-methyl-D-glucopyranoside presents three energy minima in the *gauche*−, *trans*, and *gauche*+ conformations, the *trans* rotamer being the most stable in vacuum at the present level of theory (Fig. 2f). The rotational energy profile could be well reproduced by a combination of a threefold torsional potential with phase-shift cosine +1 (favoring the three staggered conformations; force constant 9.50 kJ · mol^{-1}), and a onefold potential with phase-shift cosine −1 (favoring the *cis* conformation; force constant 9.35 kJ · mol^{-1}). These torsional potentials replace the combination of a threefold and a twofold potential (phase-shift cosines +1, force constants 5.92 and 0.418 kJ · mol^{-1}) applied to ω, and a twofold potential (phase-shift cosine +1, force constant 2.09 kJ · mol^{-1}) applied to $\tilde{\omega}$, used in the 45A3 force field.

In the case of α-*O*-methyl-D-galactopyranoside, the hydroxyl group at the C_4 position is axial in the $^4C_1$ chair conformation. This inversion at C_4 affects the interaction between the corresponding hydroxyl group and the adjacent hydroxymethyl group. As a consequence, the rotational profile around the dihedral angle $\tilde{\omega}$ is now dominated by the *gauche*− and *gauche*+ conformations (Fig. 2h). This trend could be well reproduced in the molecular-mechanical profile by using a combination of a threefold torsional potential with phase-shift cosine +1 (favoring the three staggered conformations; force constant 7.69 kJ · mol^{-1}), a onefold potential with phase-shift cosine −1 (favoring the *cis* conformation; force constant 6.66 kJ · mol^{-1}), and a onefold potential with phase-shift cosine −1 associated to the dihedral angle ω (force constant 2.67 kJ · mol^{-1}). For simplicity, it was decided to keep the torsional potential associated with χ_4 unaltered in this case, which still resulted in an appropriate fit to the corresponding quantum-mechanical profile for this dihedral angle (Fig. 2g).

As evident from Figure 2, the agreement between the quantum-mechanical and the corresponding (optimized) molecular-mechanical profiles is reasonable (especially in the low-energy regions), but by no means perfect. A closer agreement could certainly be reached by including additional terms with different multiplicities or applying distinct torsional potentials for the different χ_n ($n = 2, 3, 4, 6$) dihedral angles. However, such an improvement of the fit would probably not be justified because: (1) it would be reached at the expense of simplicity and transferability; (2) the accuracy of the present quantum-mechanical calculations is limited (basic level of theory and small basis set, limited set of configurations included); (3) solute–solvent interactions are at least as important in determining the rotamer population distributions and isomerization barriers in aqueous solution (see discussion of Figs. 3 and 4), but are themselves treated at a limited level of accuracy (point-charge model, rigid solvent geometry, no explicit inclusion of polarizability). In this sense, Figure 2 shows that the new 45A4 force field successfully captures the main trends of the quantum-mechanical rotational profiles without representing an overfitting.

The ring dihedral potentials applied in the new 45A4 force field are largely inspired from the 45A3 parameter set,[37,38] itself being almost identical to the 43A1 set[29] in the context of hexopyranoses (the only difference between 43A1 and 45A3 is that the force constant for the threefold potentials involving C–C–C–C and C–C–C–O_5 sequences of ring atoms has changed from 5.86 to 5.92 kJ · mol^{-1}). However, for hexopyranoses of the D-series, the 43A1

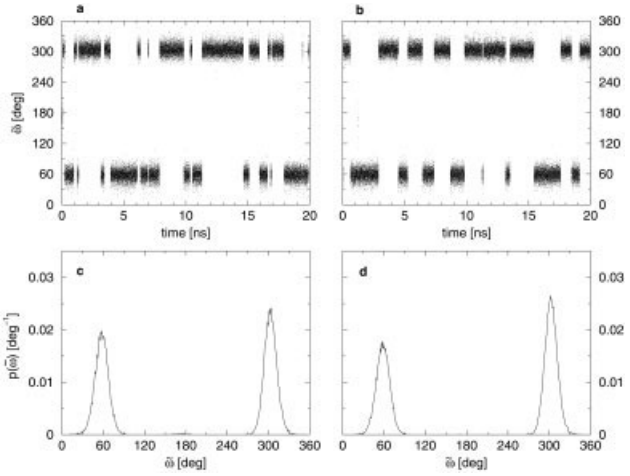

Figure 3. Time series (a,b) and normalized probability distributions (c,d) of the dihedral angle $\tilde{\omega}$ (O_5–C_5–C_6–O_6) defining the orientation of the hydroxymethyl group in α-D-glucopyranose (a,c) and β-D-glucopyranose (b,d), as obtained from 20-ns MD simulations in water (see also Table 6).

and 45A3 force fields appear to overstabilize the $^1C_4$ chair conformation relative to the (experimentally dominant, except for *D*-idopyranose[4]) $^4C_1$ conformation. This may result in undesired structural transitions between the two conformers, as previously reported in simulations using the 43A1[31,32,42,43] or 45A3 (unpublished results) parameter sets for carbohydrates. This problem was overcome by a slight modification of the scheme for the application of torsional potentials to sequences of ring atoms. The new rules applied in the 45A4 force field are the following:

1. All C–C–O_5–C dihedrals, defined by a combination of ring atoms, are assigned a threefold potential with phase-shift cosine +1 (favoring the three staggered conformations; force constant 3.77 kJ · mol^{-1}). This rule is unaltered with respect to the 45A3 force field.
2. All C–C–C–C and C–C–C–O_5 dihedrals defined by a combination of ring atoms are assigned a threefold potential with phase-shift cosine +1 (favoring the three staggered conformations; force constant 5.92 kJ · mol^{-1}). The only alteration of this rule with respect to the 45A3 force field is that it now excludes the dihedral angle C_4–C_5–C_6–O_6 (ω).
3. All O–C–C–O dihedrals not including O_5 are assigned a twofold potential with phase-shift cosine +1 (minima at 90° and 270°; force constant 2.09 kJ · mol^{-1}). This rule is modified with respect to the 45A3 force field in that it excludes the dihedral angles O_2–C_2–C_1–O_5, O_4–C_4–C_5–O_5, and O_5–C_6–C_6–O_6 ($\tilde{\omega}$).
4. All C–C–C–O dihedral angles not including O_6 are assigned a twofold potential with phase-shift cosine +1 (minima at 90° and 270°; force constant 0.418 kJ · mol^{-1}). The only alteration of this rule with respect to the 45A3 force field is that it now excludes the dihedral angle C_4–C_5–C_6–O_6 (ω).

The complete set of torsional parameters is summarized in Table 4.

The threefold ring torsional terms with phase-shift cosine +1 (rules 1 and 2) disfavor boat conformations of the ring, but do not distinguish between the $^1C_4$ and $^4C_1$ chair conformations. On the other hand, the twofold terms with phase-shift cosine +1 associated with the O–C–C–O dihedral angles (rule 3) disfavor axial–axial (180°) orientations of hydroxyl groups on vicinal carbons relative to axial–equatorial (300°) and equatorial–equatorial (60°) orientations, as a consequence of the *gauche* effect.[53–55] This interaction, in balance with nonbonded interactions around the ring and with the solvent, should result in the stabilization of the experimentally dominant $^4C_1$ chair conformation for hexopyranoses of the D-series.[4] The enhancement of the stability of the $^4C_1$ chair conformation (over $^1C_4$) in the new 45A4 force field is mostly due to the exclusion of the dihedral angles O_2–C_2–C_1–O_5 and O_4–C_4–C_5–O_5 from the twofold O–C–C–O potential (rule 3). For example, these dihedral angles both evaluate to 180° in the $^4C_1$ chair conformation of D-glucopyranose, vs. 60° and 300° in the $^1C_4$ conformation. The two potentials therefore destabilized the $^4C_1$ conformation with respect to the $^1C_4$ conformation in the 45A3 force field for this compound. Finally, the twofold terms with phase-shift cosine +1 associated with the C–C–C–O dihedral angles (rule 4) represent a very small contribution favoring chair vs. boat conformations (terms involving O_5), as well as axial vs. equatorial orientations of the hydroxyl groups in the chair conformations (terms not involving O_5).

Force Field Validation

Molecular Dynamics Simulations

A series of molecular dynamics (MD) simulations of mono- and disaccharides in water were performed so as to validate the new 45A4 parameter set by comparison against available experimental

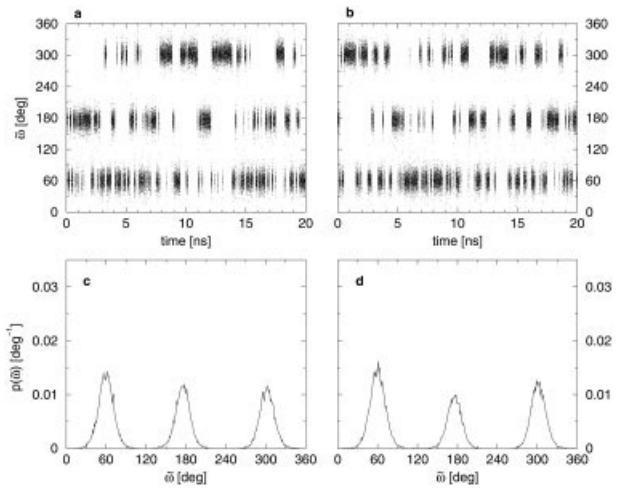

Figure 4. Time series (a,b) and normalized probability distributions (c,d) of the dihedral angle $\tilde{\omega}$ (O_5–C_5–C_6–O_6) defining the orientation of the hydroxymethyl group in α-D-galactopyranose (a,c) and β-D-galactopyranose (b,d), as obtained from 20-ns MD simulations in water (see also Table 6).

data. All simulations were carried out using the GROMOS96 program[29,35] together with the SPC water model.[36] The monosaccharides considered (α- and β-D-glucopyranose as well as α- and β-D-galactopyranose) were solvated by about 960 water molecules within a truncated-octahedral box defined by a cube of edge 3.9 nm. The disaccharides considered (trehalose, maltose, and cellobiose; the two latter as β anomer at the nonreducing center) were solvated by 2035 water molecules within a cubic computational box of edges 4.0 nm. Newton's equation of motion were integrated based on the leapfrog scheme[56] using a 2-fs time step. The SHAKE procedure[57] was applied to constrain all bond lengths with a relative geometric tolerance of 10^{-4}. The temperature was maintained at 300 K by weak coupling the solvent and solute separately to a heat bath[58] with a relaxation times of 0.1 ps. The pressure was maintained at 1.0 bar by weak coupling to a pressure bath[58] via isotropic coordinate scaling with a relaxation time of 0.4 ps. Nonbonded interactions were handled using a twin-range cutoff scheme.[59] Within a short-range cutoff radius of 0.8 nm, the interactions were evaluated every time step based on a pairlist recalculated every five time steps. The intermediate-range interactions up to a long-range cutoff radius of 1.4 nm were evaluated simultaneously with each pairlist update, and assumed constant in between. To account for electrostatic interactions beyond the long-range cutoff radius, a reaction-field approximation[60] was applied using a relative dielectric permittivity of 66 for the solvent. All simulations were carried out for 5 ns (20 ns whenever specified) after 0.1 ns equilibration, and the atomic coordinates were saved every 1 ps for analysis.

Ring Conformation

To assess the relative stabilities of the different hexopyranose ring conformations (chair or boat), a series of five 5-ns MD simulations of α-D-glucopyranose in water were undertaken, with harmonic restraining potentials on the six ring dihedral angles so as to enforce the most likely $^4C_1$, $^1C_4$, B^{14}, B^{25}, and B^{3O} ring conformations. The average intrasolute energies (i.e., including all intrasolute covalent, van der Waals, and electrostatic interactions, but excluding the dihedral-angle restraining contribution) for the different trajectories are reported in Table 5. The experimentally dominant $^4C_1$ chair conformation is clearly the most stable of all possible glucopyranose ring conformers. The energy difference between the $^4C_1$ and $^1C_4$ chair conformations (about 35 kJ $\cdot$ mol^{-1}) is also in good agreement with the corresponding range of 20–40 kJ $\cdot$ mol^{-1} obtained from quantum-mechanical calculations.[61–63] Note, however, that the second most stable conformation in the present force field appears to be the B^{3O} boat conformation rather than the $^4C_1$ chair conformation.

Interactions with the solvent are likely to largely reduce the energy differences between the different conformers in aqueous solution (and might alter their relative stabilities). To verify that the $^4C_1$ chair conformation still dominates in water, the five simulations were extended for 5 ns after releasing the dihedral-angle restraints. In the absence of restraints, the four alternative ring conformers isomerized to the $^4C_1$ chair conformation within at most 2 ns of simulation and remained in this configuration afterwards (data not shown).

Conformation of the Hydroxymethyl Group

The time series and population distributions of the dihedral angle $\tilde{\omega}$ (O_5–C_5–C_6–O_6) during 20 ns simulations of α- and β-D-glucopyranose in water are displayed in Figure 3. The corresponding relative populations of the *gt* ($\tilde{\omega} = 60°$), *tg* ($\tilde{\omega} = 180°$), and *gg* ($\tilde{\omega} = 300°$) conformers are reported in Table 6 together with experimental data from NMR.[64–68] The results may also be (qualitatively) compared to observations from X-ray crystallography[69] showing an approximate 40:0:60 ratio of *gt*:*tg*:*gg* rotamers in a survey of 101 structures involving the gluco configuration. The simulated results reproduce very well the main experimental observations, namely the very small population of the *tg* rotamer and the similar populations of the *gt* and *gg* rotamers for both α- and β-D-glucopyranose. These conformational preferences are largely influenced by solute–solvent interactions. In vacuum, the quantum-mechanical torsional profile around $\tilde{\omega}$ for α-*O*-methyl-D-glucopyranoside (Fig. 2f) presents minima of nearly equal energies in the *tg* and *gg* conformations (the former one negligibly populated in aqueous solution), while the *gt* conformation is significantly higher in energy (by about 10 kJ $\cdot$ mol^{-1}). The stability of the *tg* conformer in vacuum is largely due to an intramolecular hydrogen bond with the hydroxyl group at C_4, the hydroxymethyl group acting either as an acceptor (configuration *B* in Fig. 1, strong hydrogen bond) or as a donor (configuration *A*, weaker hydrogen bond). The absence of this conformer in solution suggests that the intramolecular hydrogen bond is wiped out by solvent effects. Note, finally, that the interconversion between the *gt* and *gg* conformers in water is relatively slow (19 and 27 transitions within the 20-ns simulation for the α- and β-anomers, respectively, counting excursions longer than 10 ps out of a well as a transition). This places the conformational relaxation of the hydroxymethyl group in glucose on the nanosecond time scale, in good agreement with experimental results from ultrasonic relaxation measurements.[70–72]

The time series and population distributions of the dihedral angle $\tilde{\omega}$ during 20-ns simulations of α- and β-D-galactopyranose in water are displayed in Figure 4. The corresponding relative populations of the *gt*, *tg*, and *gg* conformers are reported in Table 6 together with experimental data from NMR.[64–68] The results may also be (qualitatively) compared to observations from X-ray crystallography[69] showing an approximate 58:34:8 ratio of *gt*:*tg*:*gg* rotamers in a survey of 24 structures

Table 5. Average Intrasolute Energies (i.e., Including All Intrasolute Covalent, van der Waals, and Electrostatic Interactions, But Excluding the Dihedral-Angle Restraining Contribution) Calculated from Five 5-ns MD Simulations of α-D-Glucopyranose with Harmonic Restraints on the Ring Dihedral-Angles Enforcing the Specified Conformation.

Conformation	ΔE [kJ $\cdot$ mol^{-1}]
$^4C_1$	0.0
$^1C_4$	+34.8
B^{14}	+37.2
B^{25}	+71.3
B^{3O}	+20.4

Energies (ΔE) are given relative to the $^4C_1$ chair conformation.

Table 6. Relative Populations (Integrated Probability Distribution, Amplified by 100) Associated with the Three Staggered Conformations of the Hydroxymethyl Group, As Obtained from 20-ns MD Simulations of α- and β-D-Glucopyranose As Well As of α- and β-D-Galactopyranose (See Figs. 3 and 4).

$\tilde{\omega}$	α-D-Glc*p* [%]	β-D-Glc*p* [%]	α-D-Gal*p* [%]	β-D-Gal*p* [%]
60 (*gt*)	46(44[a], 54[b],53[c])	45(45[a], 62[b],61[c])	38(54[a],74[c])	41(53[a],72[c])
180 (*tg*)	0 (0[a],−1[b], 7[c])	0 (2[a],−7[b], 8[c])	31(25[a],23[c])	25(25[a],25[c])
300 (*gg*)	54(56[a], 47[b],40[c])	55(53[a], 45[b],31[c])	31(21[a], 3[c])	34(22[a], 3[c])

The three wells are defined by $\tilde{\omega}$ (O_5–C_5–C_6–O_6) in the ranges 0–120, 120–240, and 240–360°. The two letters in the notations *gt*, *tg*, and *gg* refer successively to the relative orientations of O_6 relative to O_5 (*gauche* or *trans*) and the relative orientations of O_6 relative to C_4 (*gauche* or *trans*). The values between parentheses correspond to relative populations derived from NMR experiments by [a]Nishida et al.,[64–66] [b]Brochier–Salon and Morin,[67] and [c]Thibaudeau et al.[68]

involving the galacto configuration. The simulated results reproduce well the dominance of the *gt* rotamer for both α- and β-D-galactopyranose. The similar populations observed for the *tg* and *gg* rotamers are also in good agreement with the NMR data of Nishida et al.,[64–66] but somewhat at odds with the more recent data by Thibaudeau et al.,[68] suggesting an almost negligible population for the *gg* conformer (at the benefit of the *gt* conformer). Here, also, these conformational preferences are largely influenced by solute–solvent interactions. In vacuum, the quantum-mechanical torsional profile around $\tilde{\omega}$ for α-*O*-methyl-D-galactopyranoside (Fig. 2h) presents minima of nearly equal energies in the *gt* and *gg* conformations, while the *tg* conformation is higher in energy (by about 10 kJ · mol^{-1}). In contrast to the case of glucopyranose, the axial orientation of the hydroxyl group at C_4 in galactopyranose precludes the formation of a strong intramolecular hydrogen bond between this group and the hydroxymethyl group. Yet, in water, the *tg* conformer is not populated for glucopyranose (where it could form a strong intramolecular hydrogen bond) and significantly populated for galactopyranose (where such an intramolecular hydrogen bond cannot be formed). This rather counterintuitive observation is again a hint toward a strong solvation effect on the conformational preferences of the hydroxymethyl group. Note, finally, that the interconversion between the three conformers in water is significantly faster in galactopyranose (109 and 103 transitions within the 20-ns simulation for the α- and β-anomers, respectively) compared to glucopyranose, a feature that could also be noted in previous simulations.[73] This observation may be supported by experimental results from ultrasonic relaxation measurements,[71,72] suggesting that the conformational relaxation of the hydroxymethyl group is two to four times faster in galactose compared to glucose.

The rotameric distribution for the hydroxymethyl group in α- and β-D-glucopyranose as well as α- and β-D-galactopyranose in water results from an intricate balance between: (1) the *gauche* effect (a stereoelectronic effect preferentially stabilizing *gauche* orientations of O_5 and O_6 around the C_5–C_6 bond[53–55]), which favors the *gt* and *gg* conformations in both glucose and galactose; (2) the 1,3-*syn*diaxial interaction (a steric effect destabilizing parallel orientations of the C_4–O_4 and C_6–O_6 bonds[74]), which favors the *gt* and *gg* conformations in glucose and the *gt* and *tg* conformations in galactose; (3) intramolecular hydrogen bonding (an electrostatic effect) between the hydroxyl groups at C_4 and C_6,[25,50,51,61,75,76] which favors the *tg* conformation in glucose and the *gg* conformation in galactose; (4) weak intramolecular hydrogen bonding between the hydroxyl group at C_6 and the ring oxygen O_5,[77–79] which favors the *gt* and *gg* conformations in both glucose and galactose; (5) solvation effects including the dielectric screening of intramolecular hydrogen bonds and specific solute–solvent interactions. Probably the most convincing interpretation of the rotameric populations in water[73] is that solvation effects (mainly through dielectric screening[80]) dramatically reduce the strength of intramolecular hydrogen bonding (a major contribution in vacuum,[25,50,51,61,62,75,77,81] although not necessarily the dominant one[51,61,63,81]), leaving way to the influence of steric and stereoelectronic effects[82] (together with residual intramolecular hydrogen bonding[78,79]). In glucose, both the *gauche* effect and the 1,3-*syn*diaxial repulsion favor *gt* and *gg* over *tg*. As a consequence, the latter is not significantly populated in solution. In galactose, *gg* is disfavored by 1,3-*syn*diaxial repulsion and *tg* disfavored by the *gauche* effect. As a consequence, the *gt* conformation dominates in solution, although the two other distributions (according to the NMR data by Nishida et al.[64–66]) or the *tg* distribution only (according to the NMR data by Thibaudeau et al.[68]) remain significantly populated.

Due to this delicate balance between steric, stereoelectronic, hydrogen bonding, and solvation effects, the accurate representation of the hydroxymethyl rotameric distribution in glucose and galactose is a notoriously difficult problem for classical (and Car–Parrinello) MD simulations. For this reason, it is often considered to be a challenging test for carbohydrate force fields. For example, incorrect rotameric distributions were observed in early versions of the CHARMM[17,19,83,84] and GROMOS[32,42] force fields, as well as in (comparatively shorter) Car–Parrinello simulations.[85] Taking into account the rather large uncertainty in the experimental estimates, the data reported in Table 6 indicate a very reasonable agreement with experiment.

Conformation of the Glycosidic Linkage in Disaccharides

The trajectories in the space of the ϕ (O_5–C_1–O_1–C'_1) and ϕ' (C_1–O_1–C'_1–O'_5) glycosidic dihedral angles for trehalose, or ϕ (O_5–C_1–O_1–C'_4) and ψ (C_1–O_1–C'_4–C'_3) glycosidic dihedral angles for maltose and cellobiose, during 5-ns simulations of the disac-

charides in water are displayed in Figure 5 together with available experimental data from X-ray crystallography, NMR, and circular dichroism. In the three cases, the simulations reproduce very well the ranges defined by the experimental data. Note, in particular, that the *exo*-anomeric effect dictates the predominance of $\phi = 60°$ (and $\phi' = 60°$) for the α-linked disaccharides and $\phi = 300°$ for the β-linked one.

Conclusion

The goal of the present work was to develop a new parameter set for the simulation of hexopyranose-based carbohydrates, that is compatible with the most recent version of the GROMOS force field for other classes of biomolecules[29,35,37–41] (proteins, nucleic acids, and lipids) and the SPC water model.[29,35] The parametrization procedure relied on: (1) reassigning the atomic partial charges based on a fit to the quantum-mechanical electrostatic potential around a trisaccharide; (2) refining the torsional potential parameters associated with the rotations of the hydroxymethyl, hydroxyl, and anomeric alkoxy groups by fitting to corresponding quantum-mechanical profiles for hexopyranosides; (3) adapting the torsional potential parameters determining the ring conformation so as to stabilize the (experimentally predominant) $^4C_1$ chair conformation. The other (van der Waals and nontorsional covalent) parameters and the rules for third and excluded neighbors were taken directly from the most recent version of the GROMOS force field (except for an additional exclusion between the hydroxyl hydrogen of an unfunctionalized lactol group and the ring oxygen). The updated version of the GROMOS force field, including the latest previously reported changes[37–41] and the presently derived set of carbohydrate parameters, is referred to as the GROMOS 45A4 force field. Note that a newer parameter set (53A6) has recently been developed (simultaneously with the present work), to better reproduce the hydration free energies of a set of small organic compounds presenting the most common functional groups found in biomolecules.[48] The combination of the present carbohydrate parameter set with the 53A6 force field involves a single change (slightly modified carbohydrate–oxygen to water–oxygen van der Waals repulsive interaction parameter), but remains to be tested.

The new 45A4 parameter set was validated for a small set of mono- and disaccharides in solution by comparing the results of simulations to available experimental data from X-ray crystallography and NMR spectroscopy. This validation is currently limited to α- and β-D-glucose, α- and β-D-galactose, and the disaccharides trehalose, maltose, and cellobiose. Excellent agreement was met for the ring conformation and conformer distribution of the hydroxymethyl group in monosaccharides, and for the distribution of ϕ–ψ (ϕ–ϕ') dihedral angles in disaccharides.

It should be stressed, however, that although the present description of the force field is general enough to define parameters for any (unbranched) hexopyranose-based mono-, di-, oligo-, or polysaccharide, we do not yet guarantee its accuracy for systems others than those considered in the present validation. The testing of the force field for a more extensive set of mono- and disaccharides is in progress, and the results (including possible further refinement of the parameter set) will be reported in a forthcoming article.[86]

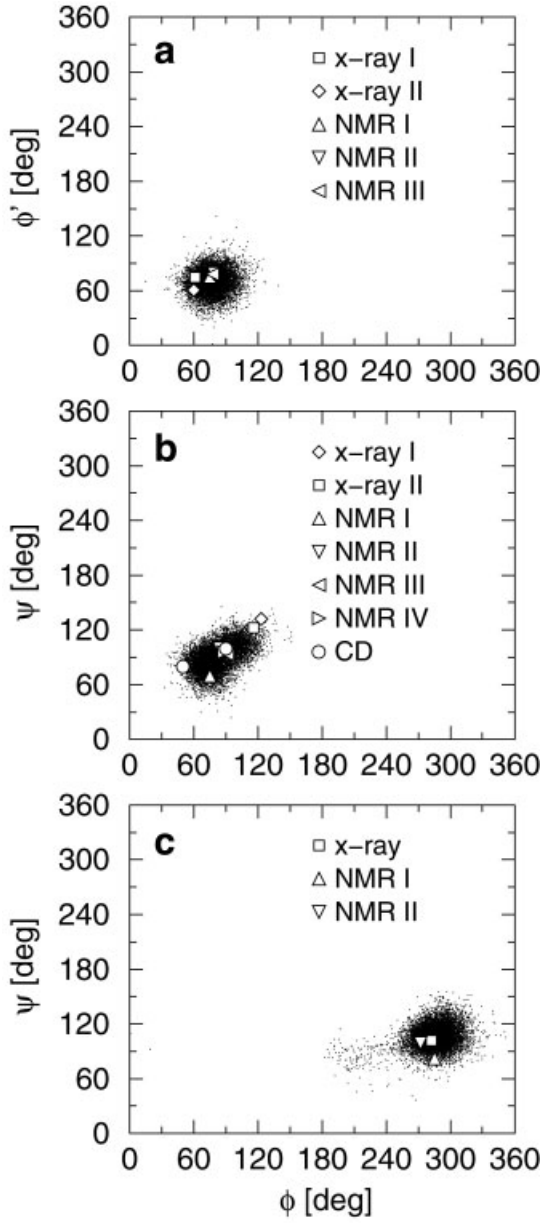

Figure 5. Trajectories in the space of the ϕ (O_5–C_1–O_1–C_1') and ϕ' (C_1–O_1–C_1'–O_5') glycosidic dihedral angles for trehalose (a), or the ϕ (O_5–C_1–O_1–C_4') and ψ (C_1–O_1–C_4'–C_3') glycosidic dihedral angles for maltose (b) and cellobiose (c), during 5-ns MD simulations of the disaccharides in water. Successive points are reported at a frequency of 1 ps. The results are compared to experimental ϕ–ϕ' or ϕ–ψ values. For trehalose: from X-ray crystallography (I: trehalose dihydrate;[91,92] II: anhydrous trehalose[93]) and three independent NMR experiments (I,[94] II,[95] and III[96]). For maltose: from X-ray crystallography (I: β-maltose monohydrate;[97] II: anhydrous α-maltose[98]), four independent NMR experiments (I,[96,99] II,[100] III,[96,101] and IV[96]), and circular dichroism.[102] For cellobiose: from X-ray crystallography[103–105] and two independent NMR experiments (I[106] and II[96]).

Note, finally, that two studies relying on of the present 45A4 carbohydrate force field have been reported.[87,88] In the first article, an early version of the force field was used to investigate the influence of methylation at specific hydroxyl groups on the stability of amylose and cellulose fragments.[87] In the second article, the parameters for trehalose were used to investigate the effect of this disaccharide on the stability of dipalmitoyl–phosphatidyl–choline lipid bilayer at elevated temperature.[88]

Acknowledgments

The authors thank Cristina Pereira, Vincent Kräutler, and Carlos Emidio for their invaluable help in testing the parameter sets at the various stages of refinement; Chris Oostenbrink for providing the results of the free-energy calculations for the ethanol model; and David Kony, Tim Heinz, and Haibo Yu for many insightful discussions. The NWChem 4.1 computational chemistry package for massive parallel computers used in this study was developed by the High Performance Computational Chemistry Group, Environmental Molecular Sciences Laboratory, Pacific Northwest National Laboratory.

References

1. Dwek, R. A. Chem Rev 1996, 96, 638.
2. Varki, A.; Cummings, R.; Esko, J.; Freeze, H.; Hart, G.; Marth, J. Essentials of Glycobiology; Cold Spring Harbor Laboratory Press: Cold Spring Harbor, NY, 1999.
3. Ramesh, H. P.; Tharanathan, R. N. Crit Rev Biotechnol 2003, 23, 149.
4. Lehmann, J. Carbohydrates Structure and Biology; Georg Thieme Verlag: Stuttgart, Germany, 1998.
5. Gabius, H. J.; Siebert, H. C.; Andre, S.; Jimenez–Barbero, J.; Rudiger, H. Chem-BioChem 2004, 5, 741.
6. Lowe, J. B.; Marth, J. D. Annu Rev Biochem 2003, 72, 643.
7. Rice, K. G.; Wu, P.; Brand, L.; Lee, Y. C. Curr Opin Struct Biol 1993, 3, 669.
8. Dwek, R. A.; Edge, C. J.; Harvey, D. J.; Wormald, M. R.; Parekh, R. B. Annu Rev Biochem 1993, 62, 65.
9. Wormald, M. R.; Petrescu, A. J.; Pao, Y.-L.; Glithero, A.; Elliott, T.; Dwek, R. A. Chem Rev 2002, 102, 371.
10. Perez, S.; Gautier, C.; Imberty, A. In Oligossaccharides in Chemistry and Biology: A Comprehensive Handbook; Ernst, B.; Hart, G.; Sinay, P., Eds.; Wiley VCH: Weinheim, Germany, 2000, p. 969.
11. Duus, J. O.; Gotfredsen, C. H.; Bock, K. Chem Rev 2000, 100, 4589.
12. Rubinstenn, G.; Sinay, P.; Berthault, P. J Phys Chem A 1997, 101, 2536.
13. Perez, S.; Kouwijzer, M. L. In Carbohydrates: Structures, Syntheses and Dynamics; Finch, P., Ed.; Kluwer Academic Press: New York, 1999, p. 258.
14. Imberty, A. Curr Opin Struct Biol 1997, 7, 617.
15. Woods, R. J. Glycoconjugate J 1998, 15, 209.
16. Mackerell, A. D., Jr. J Comput Chem 2004, 25, 1584.
17. Ha, S. N.; Giammona, A.; Field, M.; Brady, J. W. Carbohydr Res 1988, 180, 207.
18. Reiling, S.; Schlenkrich, M.; Brickmann, J. J Comput Chem 1996, 17, 450.
19. Kuttel, M.; Brady, J. W.; Naidoo, K. J. J Comput Chem 2002, 23, 1236.
20. Glennon, T. M.; Zheng, Y.-J.; Le Grand, S. M.; Schutzberg, B. A.; Merz, K. M., Jr. J Comput Chem 1997, 15, 1019.
21. Woods, R. J.; Dwek, R. A.; Edge, C. J.; Fraser–Reid, B. J Phys Chem 1995, 99, 3832.
22. Senderowitz, H.; Parish, C.; Still, W. C. J Am Chem Soc 1996, 118, 2078.
23. Simmerling, C.; Fox, T.; Kollman, P. A. J Am Chem Soc 1998, 120, 5771.
24. Momany, F. A.; Willett, J. L. Carbohydr Res 2000, 326, 194.
25. Damm, W.; Frontera, A.; Tirado–Rives, J.; Jorgensen, W. L. J Comput Chem 1997, 18, 1955.
26. Kony, D.; Damm, W.; Stoll, S.; van Gunsteren, W. F. J Comput Chem 2002, 23, 1416.
27. Kony, D.; Damm, W.; Stoll, S.; Hünenberger, P. H. J Chem Phys B 2004, 108, 5815.
28. Koehler, J. E. H.; Saenger, W.; van Gunsteren, W. F. Eur Biophys J 1987, 15, 197.
29. van Gunsteren, W. F.; Billeter, S. R.; Eising, A. A.; Hünenberger, P. H.; Krüger, P.; Mark, A. E.; Scott, W. R. P.; Tironi, I. G. Biomolecular Simulation: The GROMOS96 Manual and User Guide; Verlag der Fachvereine: Zürich, Switzerland, 1996.
30. Kouwijzer, M. L. C. E.; Grootenhuis, P. D. J. J Phys Chem 1995, 99, 13426.
31. Ott, K.-H.; Meyer, B. J Comput Chem 1996, 17, 1068.
32. Spieser, S. A. H.; van Kuik, J. A.; Kroon–Batenburg, L. M. J.; Kroon, J. Carbohydr Res 1999, 322, 264.
33. Perez, S.; Imberty, A.; Engelsen, S. B.; Gruza, J.; Mazeau, K.; Jimenez–Barbero, J.; Poveda, A.; Espinosa, J. F.; van Eyck, B. P.; Johnson, G.; French, A. D.; Louise, M.; Kouwijzer, C. E.; Grootenhuis, P. D. J.; Bernardi, A.; Raimondi, L.; Senderowitz, H.; Durier, V.; Vergoten, G.; Rasmussen, K. Carbohydr Res 1998, 314, 141.
34. Hemmingsen, L.; Madsen, D. E.; Esbensen, A. L.; Olsen, L.; Engelsen, S. B. Carbohydr Res 2004, 339, 937.
35. Scott, W. R. P.; Hünenberger, P. H.; Tironi, I. G.; Mark, A. E.; Billeter, S. R.; Fennen, J.; Torda, A. E.; Huber, T.; Krüger, P.; van Gunsteren, W. F. J Phys Chem A 1999, 103, 3596.
36. Berendsen, H. J. C.; Postma, J. P. M.; van Gunsteren, W. F.; Hermans, J. In Intermolecular Forces, in Intermolecular Forces; Pullman, B., Ed.; Reidel: Dordrecht, The Netherlands, 1981, p. 331.
37. Schuler, L. D.; van Gunsteren, W. F. Mol Simul 2000, 25, 301.
38. Schuler, L. D.; Daura, X.; van Gunsteren, W. F. J Comput Chem 2001, 22, 1205.
39. Chandrasekar, I.; Kastenholtz, M.; Lins, R. D.; Oostenbrink, C.; Schuler, L. D.; Tieleman, P. D.; van Gunsteren, W. Eur Biophys J 2003, 32, 67.
40. Soares, T. A.; Hünenberger, P. H.; Kastenholz, M. A.; Kräutler, V.; Lenz, T.; Lins, R. D.; Oostenbrink, C.; van Gunsteren, W. F. J Comput Chem 2005, 26, 725.
41. Börjesson, U.; Hünenberger, P. H. J Phys Chem B 2004, 108, 13551.
42. Klewinghaus, P.; van Eijck, B. P.; Kouwijzer, M. L.; Kroon, J. J Mol Struct Theochem 1997, 395, 289.
43. Kroon–Batenburg, L. M. J.; Kruiskamp, P. H.; Vliegenthart, J. F. G.; Kroon, J. J Phys Chem B 1997, 101, 8454.
44. Cieplak, P.; Cornell, W. D.; Bayly, C. I.; Kollman, P. A. J Comp Chem 1995, 16, 1357.
45. Woods, R. J.; Chapelle, R. J Mol Struct Theochem 2000, 527, 149.
46. Bayly, C. I.; Cieplak, P.; Cornell, W. D.; Kollman, P. A. J Phys Chem 1993, 97, 10269.
47. Harrison, R. J.; Nichols, J. A.; Straatsma, T. P.; Dupuis, M.; Bylaska, E. J.; Fann, G. I.; Windus, T. L.; Apra, E.; Anchell, J.; Bernholdt, D.; Borowski, P.; Clark, T.; Clerc, D.; Dachsel, H.; de Jong, B.; Deegan, M.; Dyall, K.; Elwood, D.; Fruchtl, H.; Glendenning, E.; Gutowski, M.; Hess, A.; Jaffe, J.; Johnson, B.; Ju, J.; Kendall, R.; Kobayashi, R.;

Kutteh, R.; Lin, Z.; Littlefield, R.; Long, X.; Meng, B.; Nieplocha, J.; Niu, S.; Rosing, M.; Sandrone, G.; Stave, M.; Taylor, H.; Thomas, G.; van Lenthe, J.; Wolinski, K.; Wong, A.; Zhang, Z. NWChem, A Computational Chemistry Package for Parallel Computers, Version 4.1; Pacific Northwest National Laboratory: Richland, WA, 2000.
48. Oostenbrink, C.; Villa, A.; Mark, A. E.; van Gunsteren, W. F. J Comput Chem 2004, 25, 1656.
49. Newsletter, Eur J Biochem 1983, 131, 1.
50. Cramer, C. J.; Truhlar, D. G. J Am Chem Soc 1993, 115, 5745.
51. Barrows, S. E.; Storer, J. W.; Cramer, C. J.; French, A. D.; Truhlar, D. G. J Comput Chem 1998, 19, 1111.
52. Frisch, M. J.; Trucks, G. W.; Schlegel, H. B.; Scuseria, G. E.; Robb, M. A.; Cheeseman, J. R.; Zakrzewski, V. G.; Montgomery, J. A., Jr.; Stratmann, R. E.; Burant, J. C.; Dapprich, S.; Millam, J. M.; Daniels, A. D.; Kudin, K. N.; Strain, M. C.; Farkas, O.; Tomasi, J.; Barone, V.; Cossi, M.; Cammi, R.; Mennucci, B.; Pomelli, C.; Adamo, C.; Clifford, S.; Ochterski, J.; Petersson, G. A.; Ayala, P. Y.; Cui, Q.; Morokuma, K.; Salvador, P.; Dannenberg, J. J.; Malick, D. K.; Rabuck, A. D.; Raghavachari, K.; Foresman, J. B.; Cioslowski, J.; Ortiz, J. V.; Baboul, A. G.; Stefanov, B. B.; Liu, G.; Liashenko, A.; Piskorz, P.; Komaromi, I.; Gomperts, R.; Martin, R. L.; Fox, D. J.; Keith, T.; Al-Laham, M. A.; Peng, C. Y.; Nanayakkara, A.; Challacombe, M.; Gill, P. M. W.; Johnson, B.; Chen, W.; Wong, M. W.; Andres, J. L.; Gonzalez, C.; Head–Gordon, M.; Replogle, E. S.; Pople, J. A. Gaussian98 (Revision A.10); Gaussian Inc.: Pittsburgh, PA, 2001.
53. Wolfe, S. Acc Chem Res 1972, 5, 102.
54. Epiotis, N. D.; Sarkanen, S.; Bjorkquist, D.; Bjorkquist, L.; Yates, R. J Am Chem Soc 1974, 96, 4075.
55. Abe, A.; Mark, J. E. J Am Chem Soc 1976, 1976, 6468.
56. Hockney, R. W. Methods Comput Phys 1970, 9, 136.
57. Ryckaert, J. P.; Ciccotti, G.; Berendsen, H. J. C. J Comput Phys 1977, 23, 327.
58. Berendsen, H. J. C.; Postma, J. P. M.; van Gunsteren, W. F.; DiNola, A.; Haak, J. R. J Chem Phys 1984, 81, 3684.
59. van Gunsteren, W. F.; Berendsen, H. J. C. Angew Chem Int Ed Engl 1990, 29, 992.
60. Tironi, I. G.; Sperb, R.; Smith, P. E.; van Gunsteren, W. F. J Chem Phys 1995, 102, 5451.
61. Barrows, S. E.; Dulles, F. J.; Cramer, C. J.; French, A. D.; Truhlar, D. G. Carbohydr Res 1995, 276, 219.
62. Csonka, G. I.; Éliás, K.; Csizmadia, I. G. Chem Phys Lett 1996, 257, 49.
63. Appell, M.; Strati, G.; Willett, J. L.; Momany, F. A. Carbohydr Res 2004, 339, 537.
64. Nishida, Y.; Ohrui, H.; Meguro, H. Tetrahedron Lett 1984, 25, 1575.
65. Ohrui, H.; Nishida, Y.; Higuchi, H.; Hori, H.; Meguro, H. Can J Chem 1987, 65, 1145.
66. Nishida, Y.; Hori, H.; Ohrui, H.; Meguro, H. J Carbohydr Chem 1988, 7, 239.
67. Brochier–Salon, M.-C.; Morin, C. Magn Reson Chem 2000, 38, 1041.
68. Thibaudeau, C.; Stenutz, R.; Hertz, B.; Klepach, T.; Zhao, S.; Wu, Q.; Carmichael, I.; Serianni, A. S. J Am Chem Soc 2004, 126, 15668.
69. Marchessault, R. H.; Pérez, S. Biopolymers 1979, 18, 2369.
70. Behrends, R.; Cowman, M. K.; Eggers, F.; Eyring, E. M.; Kaatze, U.; Majewski, J.; Petrucci, S.; Richmann, K.-H.; Riech, M. J Am Chem Soc 1997, 119, 2182.
71. Stenger, J.; Cowman, M.; Eggers, F.; Eyring, E. M.; Kaatze, U.; Pertucci, S. J Phys Chem B 2000, 104, 4782.
72. Hagen, R.; Kaatze, U. J Chem Phys 2004, 120, 9656.
73. Kirschner, K. N.; Woods, R. J. Proc Natl Acad Sci USA 2001, 98, 10541.
74. Bock, K.; Duus, J. O. J Carbohydr Chem 1974, 13, 513.
75. Ma, B.; Schaefer, H. F., III; Allinger, N. L. J Am Chem Soc 1998, 120, 3411.
76. de la Paz, M. López; Ellis, G.; Pérez, M.; Perkins, J.; Juménez–Barbero, J.; Vicent, C. Eur J Org Chem 2002, 2002, 840.
77. Brown, J. W.; Wladkowski, B. D. J Am Chem Soc 1996, 118, 1190.
78. Tvaroška, I.; Carver, J. P. J Phys Chem B 1997, 101, 2992.
79. Tvaroška, I.; Taravel, F.; Utille, J. P.; Carver, J. P. Carbohydr Res 2002, 337, 353.
80. Rockwell, G. D.; Grindley, T. B. J Am Chem Soc 1998, 120, 10953.
81. Polavarapu, P. L.; Ewig, C. S. J Comput Chem 1992, 13, 1255.
82. de Vries, N. K.; Buck, H. M. Carbohydr Res 1987, 165, 1.
83. Brady, J. W. J Am Chem Soc 1989, 111, 5155.
84. Schmidt, R. K.; Teo, B.; Brady, J. W. J Phys Chem 1995, 99, 11339.
85. Molteni, C.; Parrinello, M. J Am Chem Soc 1998, 120, 2168.
86. Pereira, C. S.; Hünenberger, P. H., in preparation.
87. Yu, H.; Amann, M.; Hansson, T.; Kohler, J.; Wich, G.; van Gunsteren, W. F. Carbohydr Res 2004, 339, 1697.
88. Pereira, C. S.; Lins, R. D.; Chandrasekar, I.; Freitas, L. C. G.; Hünenberger, P. H. Biophys J 2004, 86, 2273.
89. Riddick, J. A.; Bunger, W. B.; Sakano, T. K. Organic Solvents, Physical Properties and Methods of Purification; John Wiley and Sons: New York, 1986.
90. Wolfenden, R. Biochemistry 1981, 20, 849.
91. Brown, G. M.; Rohrer, D. C.; Berking, B.; Beevers, C. A.; Gould, R. O.; Simpson, R. Acta Crystallogr Sect B 1972, 28, 3145.
92. Taga, T.; Senma, M.; Osaki, K. Acta Crystallogr Sect B 1972, 28, 3258.
93. Jeffrey, G. A.; Nanni, R. Carbohydr Res 1985, 137, 21.
94. Poveda, A.; Vicent, C.; Penadés, S.; Jiménez–Barbero, J. Carbohydr Res 1997, 301, 5.
95. Batta, G.; Kövér, K. E.; Gervay, J.; Hornyák, M.; Roberts, G. M. J Am Chem Soc 1997, 119, 1336.
96. Cheetham, N. W. H.; Dasgupta, P.; Ball, G. E. Carbohydr Res 2003, 338, 955.
97. Quigley, G. J.; Sarko, A.; Marcheussault, R. H. J Am Chem Soc 1970, 92, 5834.
98. Takusagawa, F.; Jacobson, R. A. Acta Crystallogr Sect B 1978, 34, 213.
99. Parfondry, A.; Cyr, N.; Perlin, A. S. Carbohydr Res 1977, 59, 299.
100. Shashkov, A. S.; Lipkind, G. M.; Kochetkov, N. K. Acta Crystallogr Sect B 1986, 147, 175.
101. Pérez, S.; Taravel, F.; Vergelati, C. Nouv J Chim 1985, 9, 561.
102. Rees, D. A. In Outline Studies in Biology; Ashworth, J., Ed.; Chapman and Hall: New York, 1977, p. 1.
103. Chu, S. S. C.; Jeffrey, G. A. Acta Crystallogr Sect B 1968, 24, 830.
104. Ham, J. T.; Williams, D. G. Acta Crystallogr Sect B 1970, 26, 1373.
105. Rees, D. A.; Skerrett, R. J. Carbohydr Res 1968, 7, 334.
106. Sugiyama, H.; Hisamichi, K.; Usui, T.; Sakai, K.; Ishiyama, J. J Mol Struct Theochem 2000, 556, 173.